Journal of Statistical Physics, Vol. 43, Nos. 5/6, 1986

Simulations of the Hubbard Model

J. E. Hirsch[1]

We discuss results of simulations of the Hubbard model of interacting electrons on a lattice. We start with a brief discussion of methodology and point out some of the outstanding problems. We then discuss results of simulations of the model in three, two, and one dimension, particularly in connection with its magnetic and superconducting properties. We conclude with a brief discussion of future directions.

KEY WORDS: Magnetism; superconductivity; self-consistent field; Heisenberg model.

1. INTRODUCTION

Electrons in solids can quite generally be described in a tight binding formulation, and this formulation becomes particularly useful for "narrow-band" solids, where the kinetic energy of the electrons is comparable or smaller than their interaction energy on the average. The simplest tight-binding Hamiltonian describing interacting electrons is the Hubbard model,[1] defined by

$$H = \sum_{(i,j)} t_{ij} c_{i\sigma}^{+} c_{j\sigma} + U \sum_{i} n_{i\uparrow} n_{i\downarrow} - \mu \sum_{i,\sigma} n_{i\sigma} \tag{1}$$

where $c_{i\sigma}^{+}(c_{i\sigma})$ creates (destroys) an electron of spin σ at site i. This Hamiltonian takes into account only one atomic orbital per site and neglects interactions of electrons other than at the same site. The hopping term t_{ij} and on-site repulsion U can be expressed in terms of matrix elements of the kinetic energy operator and Coulomb interaction in the basis of atomic orbitals. One can obtain more realistic Hamiltonians by allowing for more distant interactions between electrons (extended Hub-

[1] Department of Physics, University of California, San Diego, La Jolla, California 92093.

0022-4715/86/0600-0841$05.00/0

bard model) and by considering more than one band (degenerate Hubbard model, Anderson model, etc.). Here we will limit ourselves to the form of equation (1) and only briefly consider the effect of nearest-neighbor interactions at the end.

Even in its simplest form (1), the Hubbard Hamiltonian. is thought to be useful to describe collective effects in narrow band solids such as magnetism, metal-insulator transition, and superconductivity; see, for example, Ref. 2. Because no exact solution of the model exists (except for some results in one dimension[3]), a variety of approximate methods have been used to study it,[2] whose reliability is unknown. Only recently have we started to learn about this model from Monte Carlo simulations. Besides giving information about the physics of the model, these calculations should serve as useful benchmarks against which approximate analytic methods can be tested.

The properties of the model (1) can in principle depend on the detailed form of the band structure (determined by t_{ij}), the strength of the Coulomb interaction U, the band filling, determined by the chemical potential μ, and the dimensionality. The simplest nontrivial case corresponds to half-filled band (one electron per site, or $\rho = 1$) and nearest-neighbor hopping only, for which $\mu = U/2$. For that case the dominant instability is expected to be antiferromagnetism if $U > 0$.

2. METHODOLOGY

We start with a path-integral formulation of the partition function

$$Z = \operatorname{tr} e^{-\beta H} = \operatorname{tr} \prod_{i=1}^{L} e^{-\Delta\tau H} \cong \operatorname{tr} \prod_{i=1}^{L} e^{-\Delta\tau H_o} e^{-\Delta\tau H_U} \tag{2}$$

where H_o is the kinetic energy (first term in (1)) and H_U the interaction and chemical potential terms (last two terms). Choosing $\Delta\tau^2 Ut = .125$ gives a negligible systematic error due to the breakup in (2). In one spatial dimension, inserting complete sets of intermediate states in the fermion occupation number representation between time slices leads to a sum of only positive terms that can be evaluated by standard Monte Carlo methods, taking proper account of the local spin and charge conservation laws (world line algorithm).[4] In higher dimensions, however, such a procedure leads to roughly the same number of positive and negative terms at low temperatures due to the fermion anticommutation relations,[4] and no Monte Carlo method is known to deal efficiently with this situation.

To make further progress we eliminate the electron–electron interaction term introducing auxiliary variables. Because the occupation number

$n_{i\sigma}$ can only take the values 0 or 1, this can be done by introducing one Ising variable per site[5]

$$e^{-\Delta\tau U n_{i\uparrow} n_{i\downarrow} + (\Delta\tau U/2)(n_{i\uparrow} + n_{i\downarrow})} = \tfrac{1}{2} \operatorname{tr}_\sigma e^{\lambda\sigma(n_{i\uparrow} - n_{i\downarrow})} \tag{3}$$

$$\cosh \lambda = e^{\Delta\tau U/2} \tag{4}$$

so that

$$Z = \operatorname{tr} \operatorname{tr}_\sigma \left[\prod_{l=1}^{L} e^{-\Delta\tau H_{o\uparrow}} e^{\lambda \sum_i \sigma_i(l) n_{i\uparrow}} \right] \left[\prod_{l=1}^{L} e^{-\Delta\tau H_{o\downarrow}} e^{-\lambda \sum_i \sigma_i(l) n_{i\downarrow}} \right] \tag{5}$$

Physically, the Ising variables represent the z-component of the electron spin at each site. Correlation functions of the electron spins and of the Ising variables are related by[5]

$$\langle [n_{i\uparrow}(\tau) - n_{i\downarrow}(\tau)][n_{j\uparrow}(0) - n_{j\downarrow}(0)] \rangle = \frac{1}{1 - e^{-\Delta\tau U}} \langle \sigma_i(\tau)\, \sigma_j(0) \rangle \tag{6}$$

(except for $i = j$, $\tau = 0$). We can now trace analytically over the fermion degrees of freedom in (5), since everything is bilinear in fermions. After performing this trace, the resulting theory has only two states per site (the states of the Ising spin) instead of four as the original Hubbard model. That is, our procedure can be interpreted as an exact renormalization-group transformation whereby half of the degrees of freedom (charge) are integrated out and half (spin) remains. (In fact, one can also perform a partial elimination of the charge degrees of freedom through a generalization of the transformation Eq. (3), that smoothly interpolates between the world line formulation and the Ising formulation; See Ref. 6.) As a consequence of this transformation, the sign problems that occurred in the world line formulation are completely eliminated in the half-filled band sector (the weights are positive for all σ configurations[7]), and negative signs do not cause severe problems at other band fillings, either.[8]

There are two ways to take the trce over fermion degrees of freedom in (5). In a space-only formulation one obtains[9]

$$\begin{aligned} Z &= \operatorname{tr}_\sigma \det{}_N \left[1 + \prod_{l=1}^{L} e^{\Delta\tau K} e^{V_l^\uparrow} \right] \det{}_N \left[1 + \prod_{l=1}^{L} e^{\Delta\tau K} e^{V_l^\downarrow} \right] \\ &\equiv \operatorname{tr}_\sigma \det{}_N \tilde{M}_\uparrow \det{}_N \tilde{M}_\downarrow \end{aligned} \tag{7}$$

with

$$(K)_{ij} = -t_{ij} \tag{8a}$$

$$(e^{V_l^\alpha})_{ij} = e^{\lambda\alpha\sigma_i(l)} \qquad \alpha = \pm 1 \tag{8b}$$

and $\tilde{M}_\alpha$ an $N \times N$ matrix (N = number of spatial sites). In a space-time formulation one obtains

$$Z = \mathrm{tr}_\sigma \det{}_{N,L} M_\uparrow \det{}_{N,L} M_\downarrow$$

with M_α an $(N \cdot L) \times (N \cdot L)$ matrix which, written out in the time direction, looks like

$$M_\alpha = \begin{bmatrix} e^{\Delta\tau K} e^{V_1^\alpha} & 0 & 0 \cdots & 1 \\ -1 & e^{\Delta\tau K} e^{V_2^\alpha} & 0 \cdots & \\ 0 & -1 & & \\ \vdots & \vdots & & \end{bmatrix} \tag{9}$$

If we expand the kinetic energy term or do a checkerboard breakup,[4] M_α is a sparse matrix in space-time, while $\tilde{M}_\alpha$ is a full matrix in space only.

To update the σ fields in a Monte Carlo simulation one needs the ratio of fermion determinants after and before a spin-flip, which can be written as[9]

$$\frac{\det(M + \delta M)}{\det M} = \det(1 + M^{-1}\, \delta M) \tag{10}$$

which can be easily obtained if M^{-1} is known. Because M is nonpositive definite, to use stochastic or iterative methods to obtain the inverse one needs to deal with the inverse of $M^+ M$, i.e.

$$M^{-1} = (M^+ M)^{-1} M^+ \tag{11}$$

Unfortunately, it turns out that the eigenvalue spectrum of $M^+ M$ exhibits very small eigenvalues at low temperatures.[10] For the noninteracting theory, the smallest eigenvalue of $M^+ M$ goes as

$$\lambda_{\min} \sim \left(\frac{\pi}{L}\right)^2 \tag{12}$$

as function of the number of time slices L. For the interacting case, we find numerically

$$\lambda_{\min} \sim e^{-L^{1/2}} \tag{13}$$

and for the particular case $t_{ij} = 0$ this can be proved analytically using renormalization-group arguments.[10] Equation (13) shows that the smallest eigenvalue goes to zero exponentially fast, making it very difficult to obtain $(M^+ M)^{-1}$ by stochastic or iterative methods at low temperatures. Figure 1 shows an example of the behavior of $\lambda_{\min}$ versus L for

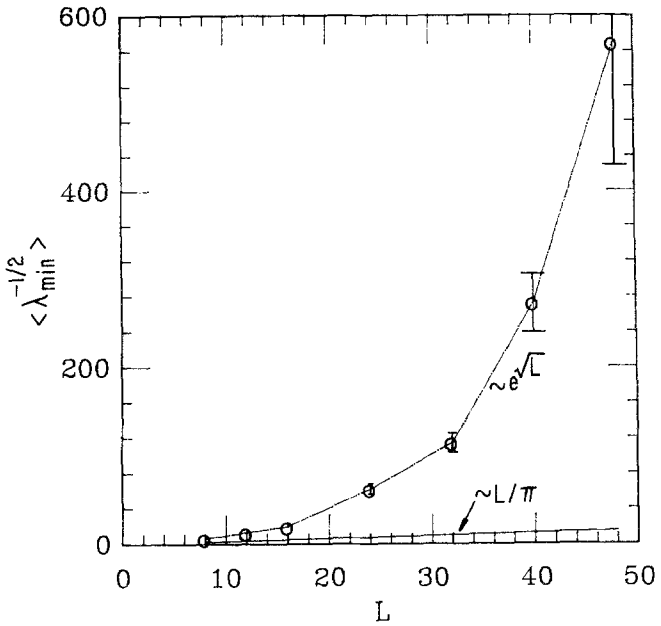

Fig. 1. Behavior of the smallest eigenvalue of M^+M, $\lambda_{\min}$, versus temperature ($L=\beta/\Delta\tau$) for $\Delta\tau U=0.5$ (upper curve) and $\Delta\tau U=0$ (lower line). Note the enormous increase in $\lambda_{\min}^{-1/2}$ produced by the random fields. The number of iterations needed to get convergence in an iterative calculation of M^+M is $\sim\lambda_{\min}^{-1}$.

fixed $\Delta\tau$. This phenomenon occurs because of a singularity in the density of states of the matrix M^+M at low energies caused by the random field configurations, and is related to the behavior found by Dyson long ago in a random chain of oscillators.[11]

This discussion shows the difficulty in obtaining the inverse of M by nondeterministic methods at low temperatures. We believe the situation is not hopeless because another feature of the matrix M^+M is that the *eigenvectors* become localized in the presence of the random field[10] so that a carefully arranged expansion starting from the inverse of a cluster can converge rapidly. This is presently being investigated.

In the absence of an efficient nondeterministic method to compute the inverse of the matrix, it is clearly advantageous to turn to the space-only formulation where the matrix $\tilde{M}$ is smaller ($N\times N$), even through nonsparse, and use a deterministic method. Blankenbecler, Scalapino and Sugar[9] have shown how one can obtain the inverse after flipping a spin in terms of the inverse before flipping the spin in $O(N^2)$ operations,[12] through the relation

$$(\tilde{M}'^{-1})_{ij}=(\tilde{M}^{-1})_{ij}+(\tilde{M}^{-1})_{ik}\,t_k(\tilde{M})^{-1}_{kj} \tag{14}$$

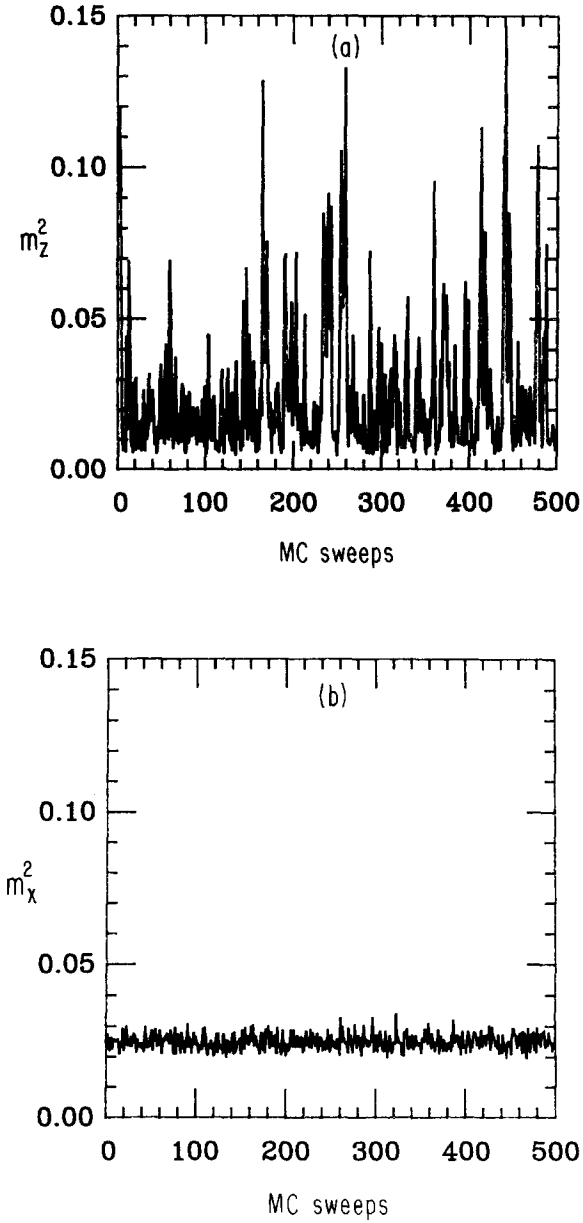

Fig. 2. Staggered magnetization squared in the z direction (a) and in the xy plane (b) versus Monte Carlo sweeps. $U = 6$, $\beta = 1.33$, 4^3 lattice. Note the much larger fluctuations in the z direction.

where t_k is the single-site t matrix, which is easily obtained. This algorithm then requires N^3L operations per sweep, i.e., is very time-consuming, but it produces reliable results. An additional difficulty is that the method becomes rapidly unstable at low temperatures and high precision is needed. We have used this approach to study the Hubbard model in two and three dimensions, and the world line formulation in one dimension. In the following sections we discuss some results.

A final technical point concerns the choice of quantities to measure. The Hubbard model is rotationally invariant in spin space, and one might think that it is inconsequential which direction in spin space one chooses to measure averages. However, the transformation (3) breaks spin-rotational invariance, and while it is restored for the *averages* on tracing over σ, it does make a big difference for the *variance*. As an example, Fig. 2 shows the staggered magnetization measured in the z direction and in the xy plane. It can be seen that the fluctuations for measurements in the xy plane are significantly smaller. This was found to be the case for all spin-dependent quantities for all cases studied.

3. RESULTS IN 3D

We have recently performed simulations of the half-filled Hubbard model in three spatial dimensions for $U \leqslant 12$ and cubic lattices of size 4^3 and 6^3. A typical simulation takes 1 Cray hr on a 4^3 lattice and 20 Cray hr on a 6^3. Figure 3 shows the local magnetic moment

$$\langle S^2 \rangle = \tfrac{3}{4}\langle (n_{i\uparrow} - n_{i\downarrow})^2 \rangle \tag{15}$$

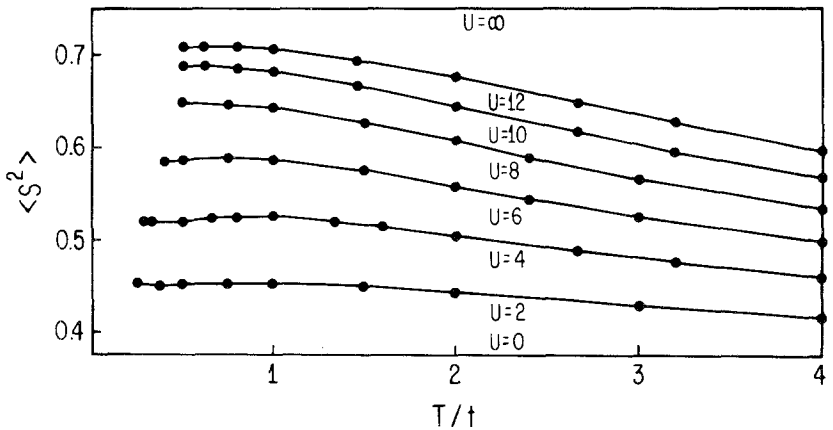

Fig. 3. Local magnetic moment (15) versus temperature for 3-D Hubbard model (4^3 lattice). The error in the MC data is smaller than the points.

versus temperature for various U. This quantity is almost independent of lattice size. For $U=0$ and $U=\infty$ the local moment is temperature-independent and equal to $\frac{3}{8}$ and $\frac{3}{4}$, respectively. For intermediate U it increases slowly as T decreases as the electrons become more localized and levels off at low T. For $U=4$ and 6 a maximum can actually be seen. For $U=12$ (bandwidth) the local moment at low T is quite close to the $U=\infty$ limit (perfectly localized spins).

Figure 4 shows spin–spin correlation functions versus U for a fixed low temperature ($\beta=0.5$). The system clearly shows antiferromagnetic correlations ($\langle S_i S_j\rangle<0$ for i, j nearest and third-nearest neighbors, and $\langle S_i S_j\rangle>0$ for next-nearest neighbors). The strongest occur around $U\sim 10$. For large U it is expected that antiferromagnetism is suppressed, since the system becomes equivalent to a Heisenberg antiferromagnet

$$H=J\sum_{\langle i,j\rangle}\boldsymbol{\sigma}_i\cdot\boldsymbol{\sigma}_j \tag{16}$$

and the exchange coupling $J=t^2/U$ decreases as U increases. For small U one expects antiferromagnetism to *increase* with U, for example, from

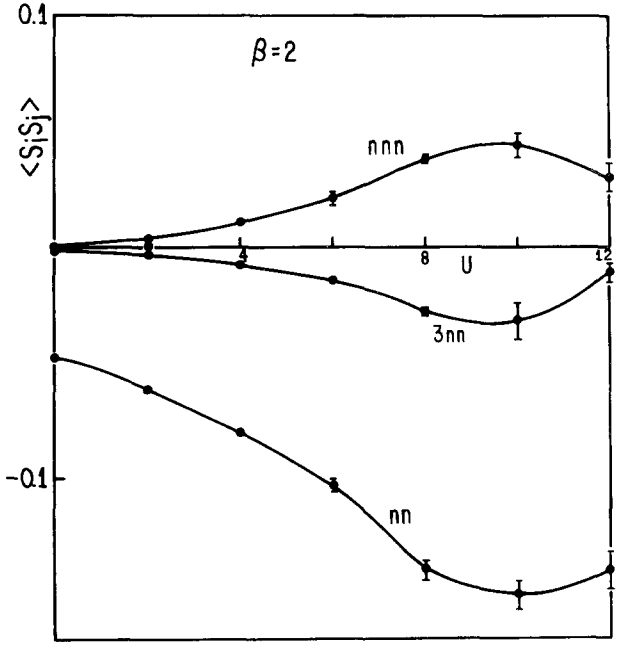

Fig. 4. Spin–spin correlation functions versus U for 3-D Hubbard model, $\beta=2$ (4^3 lattice): nn = nearest-neighbor, nnn = next-nearest neighbor, 3nn = third nearest neighbor.

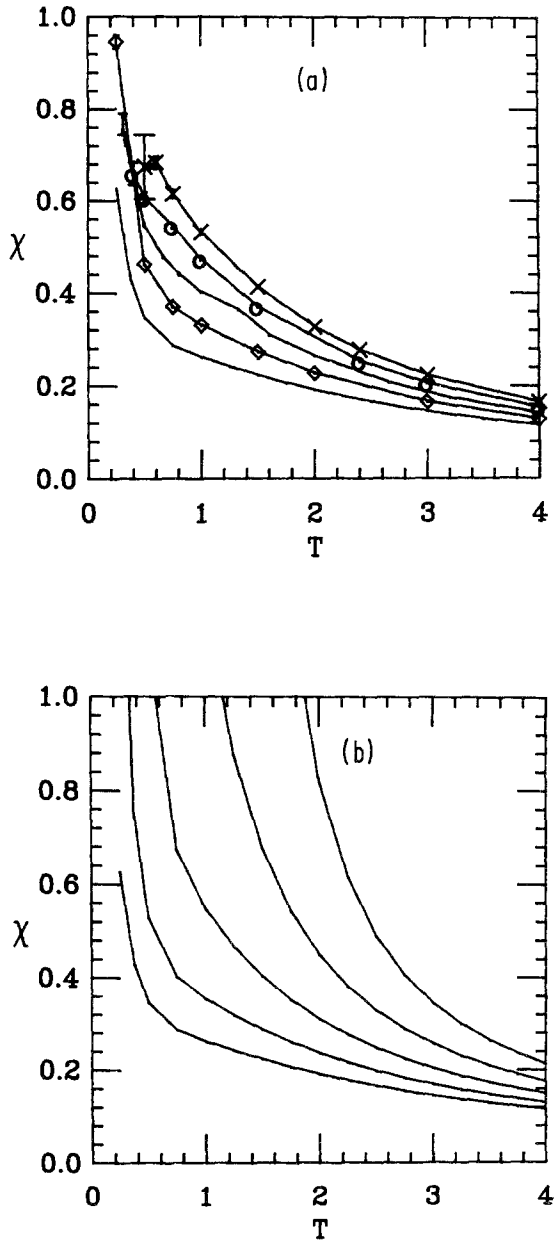

Fig. 5. (a) Magnetic susceptibility by χ versus temperature for $U=0$ (full line), $U=2$ ($\diamond$), $U=4$ ($\cdot$), $U=6$ ($\circ$) and $U=8$ (X). (b) RPA predictions.

mean-field theory. The fact that maximum antiferromagnetism occurs for $U \sim 10$, however, is new information that would be very difficult to obtain through analytic methods since it is an intermediate coupling regime.

Figure 5 shows the magnetic susceptibility for various values of U, and also the predictions of the random phase approximation (RPA). The susceptibility is enhanced by the Hubbard interaction but much less than what is predicted by RPA. We also find here that the enhancement is largest for $U \sim 10$, and a larger U starts to suppress χ (not shown) while the RPA predicts a continuous enhancement with U.

The largest effect of the interaction is seen in the magnetic structure factor and susceptibility for wavevector $\mathbf{q} = (\pi, \pi, \pi)$. As an example, Figure 6 shows $\chi(\pi)$ as a function of T for $U = 8$, which starts to increase rapidly for $T < 1$. At low temperatures the results for 2^3, 4^3, and 6^3 size lattices start to differ significantly, indicating that the system is developing long-rate antiferromagnetic order.

To determine the transition temperature T_c and the character of the transition as a function of U one could do a finite-size scaling analysis.

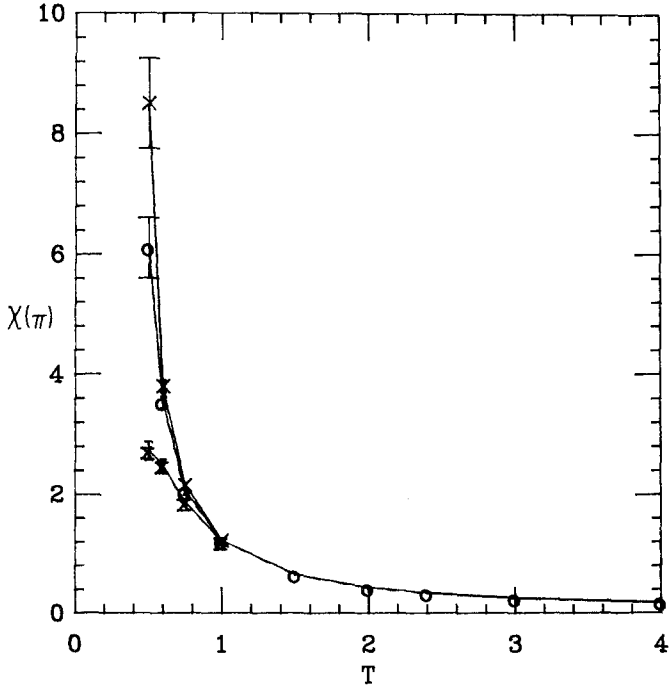

Fig. 6. Spin susceptibility at wave vector $\mathbf{q} = (\pi, \pi, \pi)$ versus temperature for $U = 8$ and lattice sizes 2^3(X), 4^3(○), and 6^3(X). For the 2^3 lattice, t is taken to be $2^{1/2}$ instead of 1. Results for the three lattice sizes are indistinguishable for $T \geqslant 1$.

Because we are limited to small lattices at present, however, this is a difficult proposition. Instead, we have used a method originally introduced by Binder[13] in a study of the classical Heisenberg model, effective field boundary conditions. The idea is to solve exactly (by simulations) for a small cluster embedded in an effective mdium to be determined self-consistently. In a mean-field decoupling scheme we have, for sites in the effective medium

$$\exp -\Delta\tau U n_{i\uparrow} n_{i\downarrow} + \frac{\Delta\tau U}{2}(n_{i\uparrow} + n_{i\downarrow}) = \exp h_i(n_{i\uparrow} - n_{i\downarrow}) \tag{17}$$

with

$$h_i = \Delta\tau U \langle n_{i\alpha} \rangle \langle -1 \rangle^{\alpha} = (-1)^i h \tag{18}$$

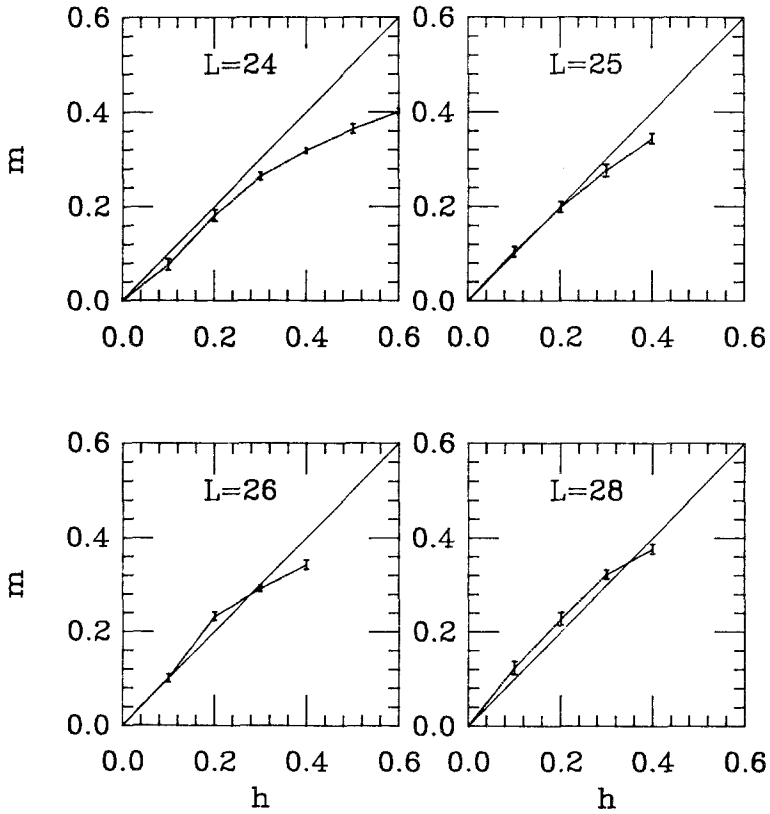

Fig. 7. Magnetization versus staggered field at the boundary for a three-site cluster embedded in a four-site cluster; $U = 4$, $\Delta\tau = 0.125$. A self-consistent nonzero solution is obtained for $L \geqslant 25$ or $\beta \geqslant 3.125$.

while for sites inside the cluster

$$\exp -\Delta\tau U n_{i\uparrow} n_{i\downarrow} + \frac{\Delta\tau U}{2}(n_{i\uparrow} + n_{i\downarrow}) = \frac{1}{2}\,\mathrm{tr}_\sigma \exp \lambda\sigma(n_{i\uparrow} - n_{i\downarrow}) \qquad (19)$$

We do the sum over σs by simulations inside the cluster, while outside we perform the decoupling (17). The mean field h_i is determined by condition (18), where $\langle n_{i\alpha}\rangle$ is the magnetization inside the cluster.

Figures 7 and 8 show results for the staggered magnetization

$$m = \sum_i (-1)^i \langle n_{i\uparrow} - n_{i\downarrow}\rangle$$

in a three-sote cluster embedded in a four-site cluster versus the mean field h for $U=4$ and $U=8$. As T is lowered, a self-consistent solution is obtained. For the larger U, in particular, it can be seen that the curve is S-shaped, which is indicative of a first-order transition.

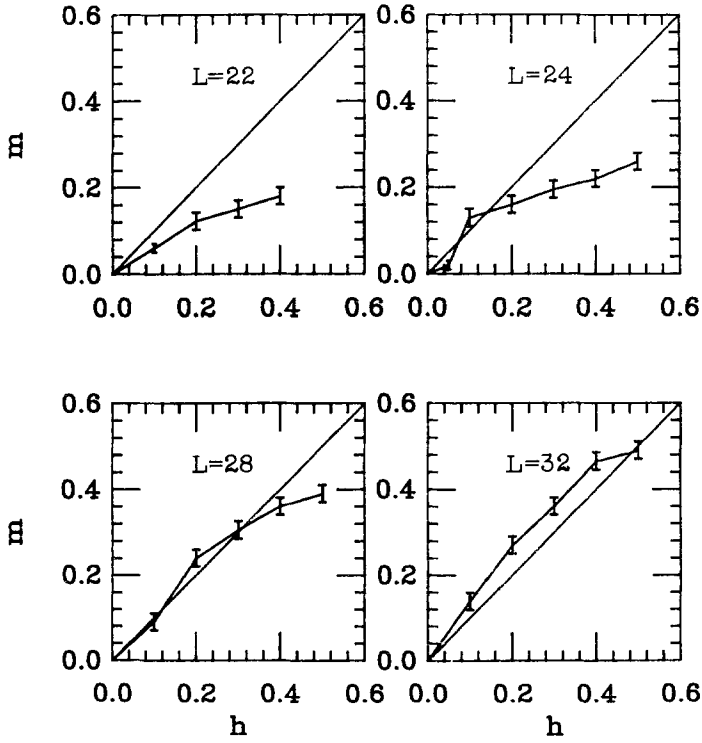

Fig. 8. Same as Fig. 7 for $U=8$ and $\Delta\tau=0.0625$.

As a check on the effective field boundary condition method, we have applied it to the three-dimensional q-state Potts model using the same size clusters as in the Hubbard simulation.[14] The results clearly show a continuous transition for $q=2$ (only one nonzero intersection in the m versus h curve) and a first-order transition for $q>2$, in accordance with known behavior.[15] It should be noted that from straight Monte Carlo simulations on these size lattices (4^3 and 6^3) it is not possible to decide that the transition is continuous for $q=2$ and first-order for $q=3$.

We have not performed a detailed analysis of the size dependence of the results with effective field boundary conditions, but estimate that our results could overestimate T_c up to 20%. For comparison, Binder's results for the 3-D Heisenberg model on a 4^3 lattice overestimate the known T_c by 14%, and our results for the $q=3$ Potts model by 23%.

Figure 9 shows the results for the critical temperature obtained in this fashion as a function of U. The RPA calculation (mean field) gives a rapidly increasing T_c with U; for large U, we plot the predictions of high temperature expansions for the $S=\frac{1}{2}$ Heisenberg model[16]; here, T_c decreases as U increases as $T_c \sim 3.36\, t^2/U$, due to the decrease in the exchange coupling J (16). The Monte Carlo results show that T_c peaks around $U \sim 10$, in accordance with the results for the spin–spin correlation functions.

An interesting feature of Fig. 9 is that the values of T_c for the Hubbard model at large U are well above the Heisenberg model predictions.

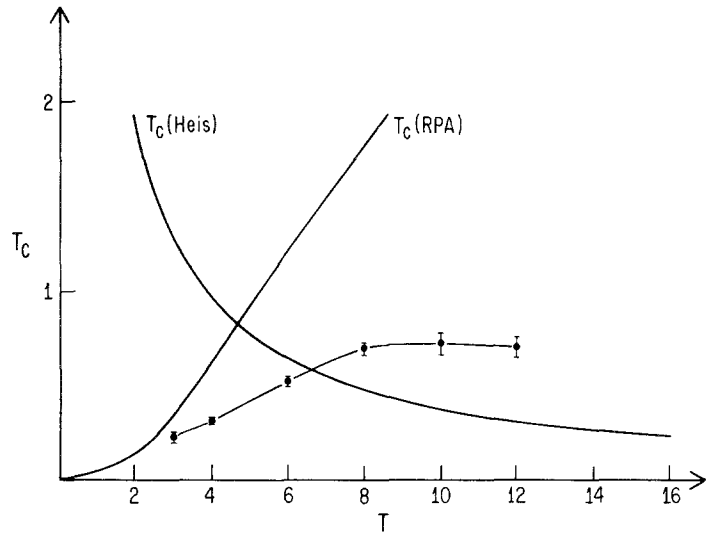

Fig. 9. Critical temperature for the paramagnetic antiferromagnetic transition in the 3-D Hubbard model versus U.

Although the Monte Carlo results probably overestimate T_c somewhat, it appears that the effect is real. This implies that when U is reduced from infinity and charge fluctuations are allowed, magnetism is actually enhanced, contrary to what one might have expected.

Finally, as mentioned before, the transition appears to be first-order for intermediate values of U. The theoretical predictions at both weak and strong coupling are for a continuous transition, which would imply the existence of two tricritical points if both the theories and the Monte Carlo results are correct in some regime. Clearly this neds to be further investigated in the future.

4. RESULTS IN 2D

In two dimensions, the Hubbard model cannot exhibit long-range order at finite temperatures since the symmetry that has to be broken (spin symmetry) is continuous. Thus, most questions of interest center around the nature of the ground state as a function of U, band filling and band structure. It is, however, also of interest to study correlation functions and

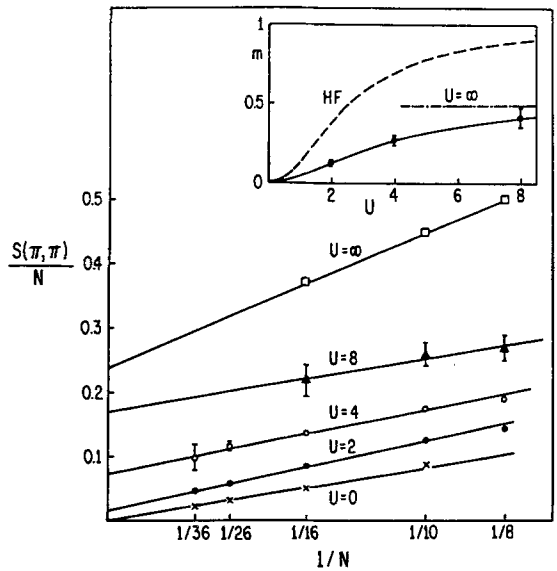

Fig. 10. Magnetic structure factor $S(\pi, \pi)/N$ plotted versus $1/N$. The extrapolation to $N \to \infty$ gives the antiferromagnetic order parameter squared, m^2. The results for $U = \infty$ correspond to the Heisenberg model and were obtained from Ref. 17. The inset shows m versus U and the Hartree–Fock predictions (HF).

susceptibilities at finite temperature since they will determine what type of order will set in in an array of weakly coupled planes (quasi-2-D system).

A variety of studies have been performed in two dimensions, and more are in progress. For the model with only nearest-neighbor hopping on a square lattice, simulations indicate that there is long-range antiferromagnetic order for all U, although substantially reduced from mean field predictions.[7,8] Some results are shown in Fig. 10.[8] For non-half-filled band cases, simulations show that there is no antiferromagnetic order for ρ as large as 0.9, suggesting that only $\rho = 1$ exhibits a magnetically ordered ground state.[8] There is also no evidence of ferromagnetism for a wide range of band fillings and interactions. Figure 11 shows the ground-state phase diagram predicted by mean-field theory and the phase diagram that emerges from simulations. Although the mean-field one exhibits a much richer structure, it unfortunately does not seem to describe the properties of the Hubbard Hamiltonian.

We have also performed studies with a modified band structure with nearest and next-nearest neighbor hopping.[18] Here, the simulations indicate that, in the $\frac{1}{2}$-filled band case antiferromagnetic, order sets in at a finite value of U, not too far from the mean-field predictions. There are ferromagnetic correlations for small lattices in the regime predicted by mean-field theory but they become weaker as the lattice size increases, and the results suggest that there is no ferromagnetism in this case either.

Concerning superconducting pairing correlations, results of simulations indicate that triplet pairing is suppressed by a repulsive interac-

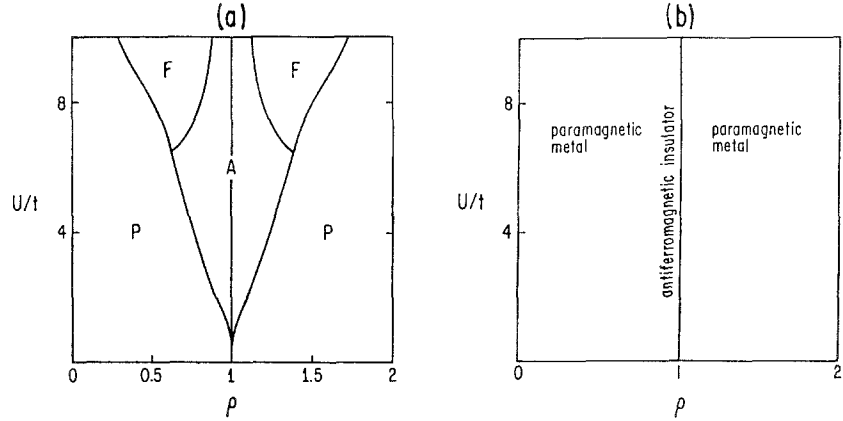

Fig. 11. Ground state phase diagram of the two-dimensional repulsive Hubbard model on a square lattice with nearest-neighbor-hopping only. (a) Mean-field prediction. A, F, and P denote antiferromagnetic, ferromagnetic, and paramagnetic phases, respectively. (b) Conjectured phase diagram from Monte Carlo results.

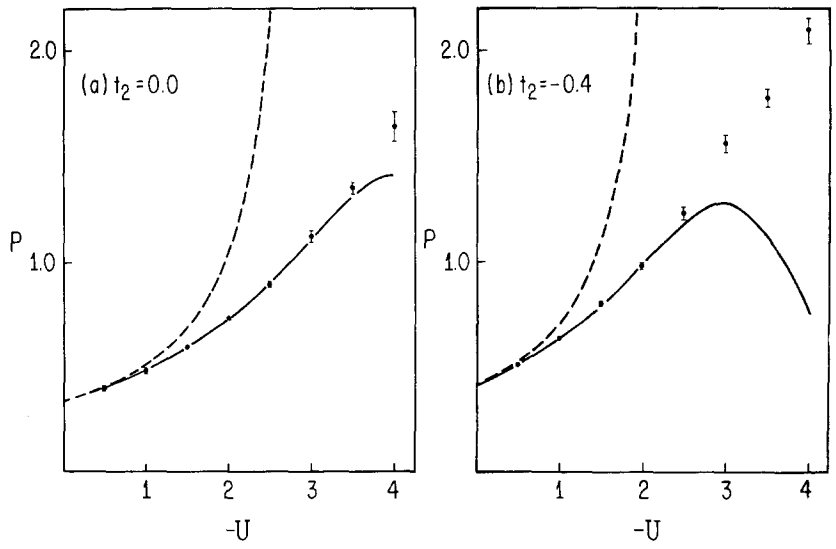

Fig. 12. Pairing susceptibility in the attractive Hubbard model versus U, indicating the tendency toward a superconducting state: 4×4 lattice, $\beta = 3$. The full line represents results obtained by summing a selected class of diagrams in perturbation theory in U for the same size lattice as the simulation results (points), the dashed line the RPA predictions. (a) Nearest-neighbor hopping only. (b) Nearest and next-nearest neighbor hopping.

tion but anisotropic singlet pairing correlations are enhanced.[8,19] These results are surprising since they are in contradiction with theoretical predictions, and may have relevance to the interpretation of the behavior of heavy fermion materials.

A detailed study of pairing correlations in the attractive Hubbard model ($U < 0$) has recently been performed.[20] Simulation results were compared with perturbation theory results obtained by summing a selected class of diagrams for small lattices. Some results are shown in Fig. 12. The theoretical calculation including the set of diagrams that gave the best agreement with Monte Carlo was then used to calculate the superconducting transition temperature as a function of U for different band structures. The results predict an enormous enhancement of the superconducting transition temperature for particular parameters, which could have important experimental consequences.

5. RESULTS IN 1D

Simulations in 1D have been performed mainly using the world-line algorithm on the Hubbard model with on-site interaction U and nearest-

neighbor interaction V. In the half-filled band case, the transition lines between charge density wave (CDW) and spin density wave (SDW) phases[21] and for the condensation transition[22] have been mapped out in detail. Figure 13 shows the results together with predictions from perturbation theory. For the CDW–SDW transition, weak and strong coupling perturbation theory predict the same transition line $U=2V$ and continuous and first-order transitions, respectively. Simulations show that the transition line deviates from the $U=2V$ line toward larger V, and that the transition is continuous for $U \lesssim 3$ and first-order beyond. For the condensation transition, strong coupling theory predicts a first-order transition in both limits $U \to \infty$ and $U \to -\infty$, and simulations show it is first-order for all values of U, and that it agrees with perturbation theory for $|U| \gtrsim 4$.

Other simulations of the 1-D Hubbard model have studied the interplay between $2k_F$ and $4k_F$ instabilities (k_F = fermi wave vector) as a function of U, V, and band filling, which is of interest in connection with X-ray diffuse scattering experiments in quasi-1-D materials.[23] Simulations showed that coexistence of $2k_F$ and $4k_F$ instabilities, as observed in some experiments, only existed in a limited range of parameters and that the $2k_F$ instability mainly appears in a *charge-transfer* susceptibility, while the $4k_F$ instability appears in the ordinary change susceptibility. This is an

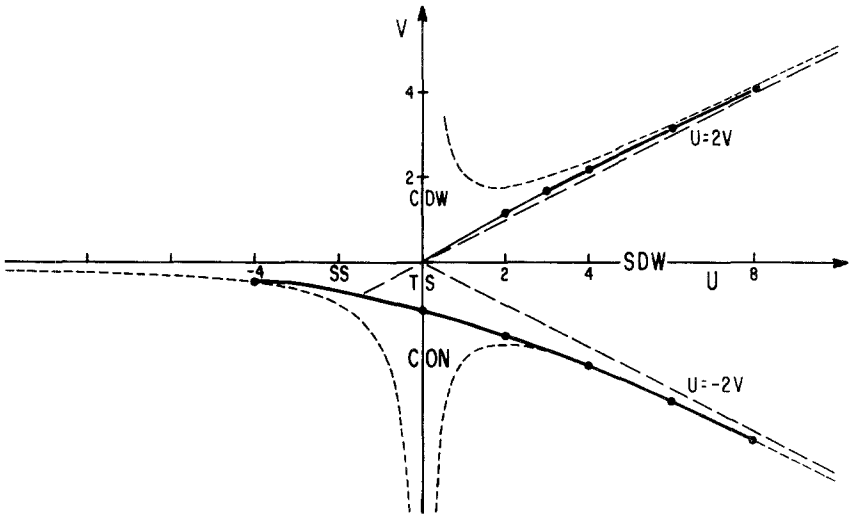

Fig. 13. Ground state phase diagram of the one-dimensional extended Hubbard model in the half-filled band sectors. The CDW–SDW transition is continuous for small U and first-order for large U ($U \gtrsim 3$), and deviates slightly from the $U=2V$ line toward the CDW phase. The condensation transition is always first-order. The dashed lines are results from various strong coupling expansions.

unexpected result of some experimental relevance since it indicates which phonon degrees of freedom couple to the instabilities. Another unexpected result was that a small on-site repulsion U can *enhance* the $2k_F$ instability, with relevance, for example, to the properties of polyacetylene.[24] Current work focuses on the effect of disorder on various instabilities in the 1D Hubbard model.

6. SUMMARY AND PROSPECTS

We have discussed some results of simulations of the Hubbard model in one, two, and three dimensions. Although the results become scarcer as we go up in dimensions, we have already learned quite a bit from simulations of this model. It is likely that simulations will allow us to gain a complete understanding of the Hubbard model, which is of interest since it is the simplest model of interacting fermions on a lattice. These results will be useful both as a reference point to understand more complicated fermion models for condensed matter systems and as benchmarks for testing approximation methods for interacting fermion systems.

Several methodological problems of course remain to be solved or improved upon. One of the most important is an efficient fermion algorithm. Although the Hubbard model looks simpler than, for example, $SU(3)$, it is in some sense more difficult, since fermions in the Hubbard model are everything, not just a perturbation on a background bose field. A "quenched approximation" would be meaningless for this model. Thus, it is likely that an algorithm that works for the Hubbard model will work for almost everything else, but that some algorithms that are useful, for example, in $SU(3)$ cannot be applied to the Hubbard model. There are at present several fermion algorithms and new ones are being developed, and a critical comparison between algorithms needs to be performed.

Other technical problems concern the difficulty of getting to very low temperature and very strong couplings, and that fact that negative fermion determinants do occur for non-half-filled band cases. Hopefully, progress in these aspects will also occur.

If we remember that only 5 years ago the only known way to obtain reliable numerical answers for the Hubbard model was through exact diagonalization, which for a 64-site Hubbard model would take $\sim 10^{20}$ Cray hr, it is clear that significant progress has occurred (simulations for 64 sites take ~ 1 Cray hr). It is likely that significant progress will continue in the next 5 years, although perhaps not at quite the same rate.

ACKNOWLEDGMENTS

This work as supported by the National Science Foundation under grant No. DMR-82-17881. In addition, the author is grateful to the Alfred P. Sloan Foundation for a research fellowship, and to Exxon Corporation and Cray Research for their support. The simulations on the 3-D Hubbard model were performed on a Cray 1 at the University of Minnesota through a grant of the OASC at NSF.

REFERENCES

1. J. Hubbard, *Proc. Roy. Soc. London A* **276**:283 (1963); **281**:401 (1964).
2. T. Moriya, ed., Electron Correlation and Magnetism in Narrow-Band Systems, (Springer, New York, 1981).
3. E. Lieb and F. Wu, *Phys. Rev. Lett.* **20**:1445 (1968).
4. J. E. Hirsch, D. J. Scalapino, R. L. Sugar, and R. Blankenbecler, *Phys. Rev. B* **26**:5033 (1982).
5. J. E. Hirsch, *Phys. Rev. B* **28**:4059 (1983).
6. J. E. Hirsch, to be published.
7. J. E. Hirsch, *Phys. Rev. Lett.* **53**:2327 (1984).
8. J. E. Hirsch, *Phys. Rev. B* **31**:4403 (1985).
9. R. Blankenbecler, D. J. Scalapino, and R. L. Sugar, *Phys. Rev. D* **24**:2278 (1981); D. J. Scalapino and R. L. Sugar, *Phys. Rev. B* **24**:4295 (1981); *Phys. Rev. Lett.* **46**:519 (1981).
10. J. E. Hirsch (unpublished).
11. F. T. Dyson, *Phys. Rev.* **92**:1331 (1953).
12. See also, D. Ceperley, G. V. Chester, and M. W. Kalos, *Phys. Rev. B* **16**:3081 (1977).
13. K. Binder, *Phys. Lett. A* **30**:273 (1969); H. Müller-Krumbhaar and K. Binder, *Z. Physik* **254**:269 (1972).
14. J. E. Hirsch (unpublished).
15. F. Y. Wu, *Rev. Mod. Phys.* **54**:235 (1982).
16. G. S. Rushbrooke, G. A. Baker, Jr., and P. J. Wood, in *Phase Transitions and Critical Phenomena*, Vol. 3, C. Domb and M. S. Green, eds. (Academic Press, New York), p. 245.
17. J. Oitmaa and D. Betts, *Can. J. Phys.* **56**:897 (1978).
18. H. Q. Lin and J. E. Hirsch, to be published.
19. J. E. Hirsch, *Phys. Rev. Lett.* **54**:1317 (1985).
20. J. E. Hirsch and D. J. Scalapino, to be published.
21. J. E. Hirsch, *Phys. Rev. Lett.* **53**:2327 (1984); *Phys. Rev. B* **31**:6022 (1985).
22. H. Q. Lin and J. E. Hirsch, *Phys. Rev. B* (to be published).
23. J. E. Hirsch and D. J. Scalapino, *Phys. Rev. Lett* . **50**:1168 (1983); *Phys. Rev.* **B27**:7169 (1983); *Phys. Rev. B* **29**:5554 (1984).
24. J. E. Hirsch, *Phys. Rev. Lett.* **51**:296 (1983).